Organic Electronics 13 (2012) 885–893

Contents lists available at SciVerse ScienceDirect

Organic Electronics

journal homepage: www.elsevier.com/locate/orgel

Spectroscopic ellipsometry characterization of vacuum-deposited organic films for the application in organic solar cells

D. Wynands [a,*], M. Erber [a], R. Rentenberger [a], M. Levichkova [b], K. Walzer [b], K.-J. Eichhorn [a], M. Stamm [a]

[a] Leibniz-Institut für Polymerforschung Dresden e.V., Hohe Str. 10, 01069 Dresden, Germany
[b] Heliatek GmbH, Treidlerstraße 3, 01139 Dresden, Germany

ARTICLE INFO

Article history:
Received 15 September 2011
Received in revised form 15 January 2012
Accepted 29 January 2012
Available online 19 February 2012

Keywords:
Ellipsometry
VASE
Anisotropy
Vacuum-deposition
Organic thin films
Solar cell

ABSTRACT

Variable angle spectroscopic ellipsometry (VASE) in the wavelength range from 245 to 1680 nm has been applied to determine the optical properties of the recently developed electron donor α,ω-bis-dicyanovinylene-sexithiophene (DCV6T), an efficient absorber material in organic solar cells (OSCs). To ensure uniqueness of the evaluation results interference enhanced substrates are used and comparison to simple native silicon substrates is presented. Similar as applied in OSC, DCV6T was deposited both as a pure single layer as well as in a mixed heterojunction with C60. For both cases, the in-plane refractive indices and extinction coefficients were higher than the out-of-plane ones, revealing that the DCV6T molecules in the films are preferentially horizontally oriented. This rough indication was further quantified by the so called molecular orientation parameter. Moreover, it is shown that annealing initiates molecular reorganization of the films, which leads to a higher birefringence and more defined horizontal orientation in the single layer. However, in the mixed layer annealing seems to reduce anisotropy. These effects and the consequences for the performance of organic solar cells are discussed.

1. Introduction

Vacuum-deposited organic films are meanwhile widely applied in organic electronic and optoelectronic devices such as organic solar cells (OSCs), high efficiency organic light-emitting diodes (OLEDs) or organic field-effect transistors (OFETs) [1–7]. Advantages like accurate thickness control, high material purity, stacking of multi-layer systems, and the opportunity of using flexible substrates make them attractive for a wide range of applications and large scale fabrication.

The electrical and optical properties of organic materials have been widely investigated to improve the performance of organic electronics. However, these properties are most often not yet fully clarified due to the large number of substances, the complexity of materials, effects of impurities, molecular conformation and aggregation. In particular the molecular order is often found to strongly influence properties like e.g. charge transport. In OFETs efficient operation relies on overlapping π-electron systems of adjacent molecules, ideally standing upright relative to the underlying substrate, thus providing high charge carrier mobility in the direction parallel to the substrate. In contrast, OSC work most efficiently when high mobility in vertical direction is achieved, e.g. by flat lying molecules, which allow π-stacking perpendicular to the substrate plane. Additionally, in OSCs flat lying molecules also enable good interaction of the transition dipole with the incident electromagnetic light wave. Consequently, the investigation and understanding of molecular orientation is essential for further improving various kinds of organic electronic devices. Usually the molecular orientation is found to be resulting from the crystal structure

* Corresponding author.
E-mail address: wynands@physics.ucsb.edu (D. Wynands).

1566-1199/$ - see front matter © 2012 Elsevier B.V. All rights reserved.
doi:10.1016/j.orgel.2012.01.036

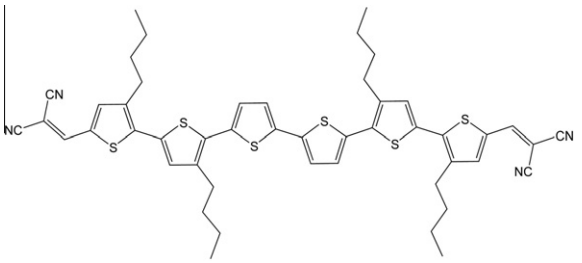

Fig. 1. Chemical structure of the α,ω-bis-dicyanovinylene-sexithiophene derivative DCV6T-Bu(1,2,5,6) (DCV6T).

and the common assumption is that amorphous vacuum-deposited organic films would be isotropic (random). However, Yokoyama et al. reported recently that linear or planar shaped molecules, which form amorphous films, are preferentially horizontally oriented and that the longer the molecular length is, the larger the anisotropy of the alignment becomes – an effect similar to nematic liquid crystals [8–10]. Yokoyama et al. successfully applied variable angle spectroscopic ellipsometry (VASE) for their experiments. In previous reports we also showed that VASE in the visible and mid-infrared spectral wavelength regions can be used to determine the optical anisotropy in thin films of linear macromolecules [11,12].

In this article, we demonstrate exemplarily by VASE why the recently introduced α,ω-bis-dicyanovinylene-sexithiophene derivative DCV6T-Bu(1,2,5,6) (DCV6T) is an efficient absorber in OSC [13,14]. The corresponding chemical structure is given in Fig. 1. The molecule comprises butyl side chains at the thiophene units number 1, 2, 5, and 6, respectively. We study both pure films of DCV6T, and DCV6T:C60 mixtures, i.e. DCV6T layers as used in either flat heterojunction or bulk heterojunction organic solar cells. By measuring the optical constants with VASE, and in particular by evaluation of the optical anisotropy, the molecular orientation of DCV6T in the thin films may be quantified. We demonstrate that anisotropy can also be detected in mixed DCV6T:C60 layers, showing that VASE is a powerful tool to increase the understanding of mixed layer morphology, a fact that is up to now not well represented in literature. As is known from experiments with OSC, annealing of the absorber layer, or deposition onto heated substrates often improves the photovoltaic properties of the absorber [15–18]. Therefore, we finally study the change of molecular arrangement upon annealing of the layers to 90 °C. This temperature was found to result in optimal device performance when using substrate heating during layer deposition [13].

In order to achieve reliable results, i.e. unique set of parameters that fit the ellipsometric measurement, we utilize interference enhanced substrates and present a comparison to the commonly used native silicon substrates.

2. Methods

2.1. Spectroscopic ellipsometry

VASE measures the polarization change of light that is reflected from a sample. This change results from the different complex Fresnel coefficients for reflection of the *P* and *S* polarized components: R_P and R_S. It is expressed by the ellipsometric angles Ψ and Δ as

$$\rho = \tan(\Psi)e^{i\Delta} = \frac{R_P}{R_S}, \tag{1}$$

where Ψ describes the amplitude ratio and Δ the phase difference. A detailed discussion of ellipsometry can be found in several textbook references [19,20].

By measuring Ψ and Δ at different angles of incidence the optical constants and film thickness of the sample layers can be determined. However, this is not a straight forward calculation but the sample structure must be modeled and the model-generated data is compared to the experimental result, while the parameters, e.g. optical constants or film thickness are varied. Within this iteration process the model, which matches the experimental values best, is found by minimizing the mean square error (MSE)

$$MSE^2 = \frac{1}{2N-M}\sum_{i=1}^{N}\left[\left(\frac{\Psi_i^{\mathrm{mod}}-\Psi_i^{\mathrm{exp}}}{\sigma_{\Psi,i}^{\mathrm{exp}}}\right)^2+\left(\frac{\Delta_i^{\mathrm{mod}}-\Delta_i^{\mathrm{exp}}}{\sigma_{\Delta,i}^{\mathrm{exp}}}\right)^2\right], \tag{2}$$

where σ^{exp} are the experimental error bars, *M* is the number of fit parameters, and *N* is the number of measured $\Psi-\Delta$ pairs.

Evaluation of the model should not rely on a good MSE alone, but it is also necessary to prove the accuracy and the uniqueness of the result when good matching to the experiment is found. For example, when too many parameters are applied, correlation can occur. Two correlated parameters cannot be determined independently but provide multiple sets of solutions, giving similar quality of the overall fit. Thus, the result is not unique. Parameter correlation can be checked by determining the two parameter correlation coefficients

$$S_{jk} = \frac{C_{jk}}{\sqrt{C_{jj}}\sqrt{C_{kk}}}, \tag{3}$$

where c_{jk} are the elements of the covariance matrix of the fitting parameters. High parameter correlation is then indicated by values close to −1 or 1.

Another way to evaluate if the result is correct, is the uniqueness test. In this test, a certain parameter under question is fixed at a series of values, while the fitting procedure determines the best set of all other parameters minimizing the MSE. From the development of the resulting MSE values, the sensitivity of the result on the tested parameter can be checked.

In principle ellipsometric measurements at several angles of incidence are sufficient to determine the film thickness and the anisotropic (uniaxial) optical properties (in-plane and out-of-plane) of absorbing organic films. However, in practice the fitting process may tend to diverge, leading to high correlation among fitting parameters and low reliability [21,22]. Checking the uniqueness of the result is therefore indispensable, especially when anisotropic optical models are applied, which are basically increasing the number fit parameters.

Different experimental approaches exist to overcome such problems by gaining more information content, thus

reducing correlations. The main three possibilities are: (a) reflection ellipsometry in combination with transmission ellipsometry [21–24], (b) multi-sample analysis [22,23] and (c) interference enhanced ellipsometry [22,23,25]. The combination between ellipsometry and transmission is helpful to reduce the parameter correlation. However, this method requires transparent substrates, and both transmission and reflection intensity values must be accurately measured. On the other hand, multiple sample analysis requires identical optical constants of different thick samples. Since the film microstructure of organic materials can vary with thickness this assumption is not always valid. In this work, we apply the latter approach, i.e. interference enhanced ellipsometry. The primary function of interference enhancement, is to significantly change the path length of light interacting with the sample at multiple angles of incidence, thus providing new information.

3. Experimental

The VASE investigations were performed using a spectroscopic ellipsometer (M2000 UI, J.A. Woollam Co., Inc.) at three different angles of incident light ranging from 55° to 75° in steps of 10°. At each angle of incidence the ellipsometric angles Ψ and Δ were measured throughout the spectral region from 245 to 1680 nm. The values of Ψ and Δ did not change when rotating the samples in the horizontal xy-plane, showing that no in-plane anisotropy is present. Thus the samples are either isotropic or uniaxial anisotropic with the optical axis perpendicular to the substrate surface. The analysis of the measured data was performed using the WVASE32 software from J.A. Woollam Co., Inc. which benefits from the Levenberg–Marquardt algorithm for fitting. The optical models were determined consecutively in several steps.

At first, the optical constants and the thickness were fitted in the transparent wavelength region above 1000 nm using an isotropic optical model, where the extinction coefficient k is equal to zero and the wavelength dependence of the refractive index n can be adequately described by the Cauchy equation given as:

$$n(\lambda) = A + \frac{B}{\lambda^2} + \frac{C}{\lambda^4}. \tag{4}$$

If necessary, e.g. in DCV6T, an uniaxial anisotropic model in the transparent region is applied with two Cauchy components representing the refractive index in-plane and out-of-plane. The decision to choose either an isotropic or an anisotropic model was reached with respect to the corresponding MSE values.

In the second step, the film thickness d was fixed and n and k were allowed to vary independently across the entire spectral range to fit the ellipsometric data (point-by-point-fit). In order to reach results, that fullfill Kramers–Kronig consistency, we finally used an harmonic oscillator approach (several Gaussian, Lorentz and Tauc–Lorentz oscillators), thus ensuring to observe physically reliable results [19,20]. In this approach the point-by-point fit results are used as a first guess starting point. When anisotropy is taken into account, the energetic positions of the oscillators in-plane and out-of-plane components have been coupled, in order to reduce the number of fit parameters. Since energetic shifts between in-plane and out-of-plane components of the absorption bands are not expected, this approach seems reasonable. We have also tested fits with fully free parameters, but did not achieve significant improvements of the MSE by decoupling the energetic positions.

The uniaxial anisotropy of the samples is evaluated by different parameters. Anisotropic samples exhibit birefringence, i.e. different refractive index in ordinary (in-plane) and extraordinary (out-of-plane) direction to the optical axis. Furthermore, the in-plane and out-of-plane extinction coefficients will differ considerably due to the difference in polarization strength, depending on the orientation of the molecular transition dipole moment. This is expressed in the ratio of the extinction coefficients $k_{\text{in-plane}}/k_{\text{out-of-plane}}$. The orientation order can be evaluated by the corresponding parameter

$$S = P_2(\cos\theta) = \frac{1}{2}\langle 3\cos^2\theta - 1\rangle = \frac{k_{\text{out-of-plane}} - k_{\text{in-plane}}}{k_{\text{out-of-plane}} + 2k_{\text{in-plane}}}, \tag{5}$$

where θ is the angle between the molecular transition dipole and the direction perpendicular to the substrate surface, $\langle \ldots \rangle$ is the ensemble average and $P_2(x)$ is the second Legendre polynomial. $S = -0.5$ denotes a perfectly parallel to the substrate ordered orientation of the molecular transition dipole, while $S = 1$ denotes a perfect perpendicular orientation. $S = 0$ when there is either no order, i.e. random orientation, or all transition dipoles are perfectly oriented in a 54.7° angle. Here, the ensemble average tilt angle θ is determined from the measured maximum extinction coefficients of the respective absorption features [8]. Estimation of the measuring error is done by evaluation of the 10% uniqueness range of the in-plane and out-of-plane extinction coefficient peak values individually [22].

As substrates, we used silicon wafers with different SiO_x layer thickness of either 2.5 nm (native silicon substrate) or 964 nm (interference enhanced substrate). Cleaning of the substrates was done using sonication in aqueous detergent, acetone, ethanol and finally isopropanol.

The organic thin films were prepared by thermal vacuum-deposition in a vacuum chamber with base pressure of about 10^{-8} mbar. Film thickness was controlled using a quartz crystal microbalance that has been calibrated before deposition by placing a second crystal at the position of the sample. Deposition rates of 0.1–0.4 Å/s have been used. Mixed layers of DCV6T:C60 were prepared by co-evaporation.

Three samples A, B, and C with single layers of DCV6T (chemical structure: see Fig. 4) were made on native silicon substrates, using layer thicknesses of 47, 98, and 136 nm, respectively. These are compared to sample D, comprising a 116 nm thick DCV6T layer deposited on an interference enhanced substrate (964 nm SiO_x on silicon). Sample D was measured at four different angles of incidence varying from 60° to 75° in 5° steps. An interference enhanced substrate is also used for investigation of the mixed

DCV6T:C60 layer, i.e. sample F. The mixed layer has a thickness of 88 nm and the DCV6T:C60 ratio is 2:1 by volume. Furthermore, in sample E, we studied a 50 nm thick layer of C60 on native silicon substrate, in order to compare the optical properties of the pure material with those of the mixed layer.

To investigate the effect of annealing, sample D (116 nm DCV6T) and F (88 nm DCV6T:C60) were annealed at 90 °C for 120 min, using a closed heat cell, which has been flushed with argon prior to the annealing. By this, oxidation reactions which could in fact influence the film morphology should be prevented.

Ellipsometric measurements usually require that the investigated films are very smooth. Therefore, the surface morphology of the samples was characterized by atomic force microscopy (AFM) using a Digital Instrument Nanoscope IIIa in tapping mode. By this, the roughness of the samples is checked and thus the accuracy of the ellipsometric model evaluation is ensured.

4. Results and discussion

4.1. Effect of interference enhanced substrates

Fig. 2 shows uniqueness tests of the fit parameter thickness (d) for samples A, B, and C, comprising DCV6T layers with a thickness of 47, 98, and 136 nm, respectively, on native silicon substrates. These tests were carried out using the anisotropic Cauchy model in the wavelength range of 1000–1680 nm.

Especially in sample A, we observe very low sensitivity of the MSE with d, thus showing that the resulting parameters are not unique. As the DCV6T layer thickness increases in samples B and C, more unique results are achieved. This is also reflected in the development of the maximum correlation matrix value (3) between d and the other parameters. It is 0.997, and thus very high, in sample A, but decreases to 0.907 in sample B, and finally to 0.891 in sample C. Obviously, increasing the thickness of the organic layer helps to obtain more reliable ellipsometric results. However, a further improvement of the uniqueness without utilizing organic layer thickness well above 100 nm is desirable, because in application, e.g. solar cells, usual film thicknesses are below 100 nm.

Therefore, in sample D we apply interference enhanced ellipsometry, incorporating a thick dielectric layer (964 nm SiO_x) on top of the silicon substrate, while the DCV6T layer thickness is 116 nm. As can be seen in Fig. 2, the uniqueness of the obtained thickness fit is significantly enhanced compared to the native silicon oxide substrates. Furthermore, under these experimental conditions a maximum correlation matrix value between d and the other parameters of 0.528 is observed, i.e. parameter coupling is further reduced compared to the native silicon substrates. As can be seen in Fig. 3, in the wavelength range where the organic DCV6T layer is transparent, the interference effect leads to well pronounced oscillatory features in the ellipsometric angles Ψ and Δ. These oscillations differ for each angle of incidence, and thus provide higher information content.

This example shows, that the interference enhancement method is highly suited for investigation of thin organic films. Especially, when anisotropic materials are studied,

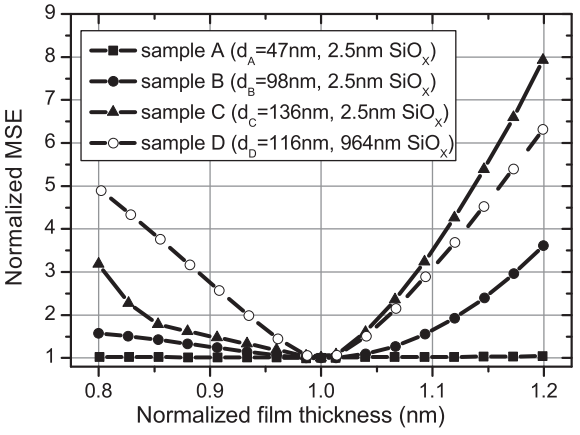

Fig. 2. Uniqueness tests for the parameter film thickness (d) performed for samples A, B, and C, comprising single DCV6T layers of varying thickness deposited on native silicon substrates. Furthermore, the same uniqueness test is shown for sample D, with 116 nm DCV6T grown on interference enhanced substrate. In these tests an anisotropic Cauchy model was used in the wavelength range of 1000–1680 nm, where the material is transparent.

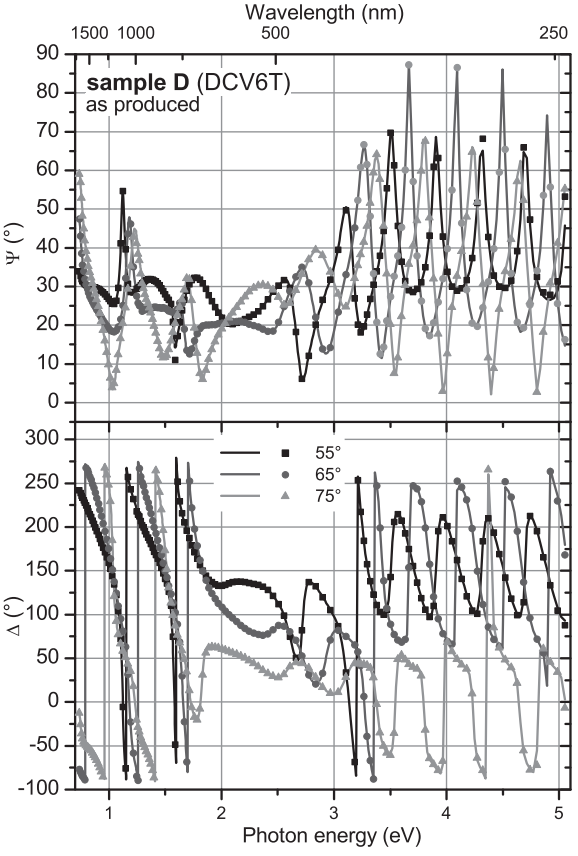

Fig. 3. Comparison between fit data (lines) and measured Ψ and Δ values (symbols) for sample D, comprising a single DCV6T layer on interference enhanced substrate.

the ellipsometric investigations benefit from the thick dielectric layer and reliable results can be obtained.

4.2. Single layers DCV-6T

In Fig. 4 the optical constants of the single layer DCV6T, measured at sample D, are presented. We observe uniaxial anisotropy according to the comparison of the MSE between the anisotropic and isotropic model approaches given in Table 1. The in-plane extinction spectrum resembles the thin film absorption of DCV6T given in Ref. [13] and shows a broad absorption band from 350 to 700 nm with distinct vibronic substructure. The out-of-plane extinction is significantly smaller and a strong birefringence of $\Delta n = 0.139$ at 1200 nm can be deduced, denoting the optical anisotropy of the DCV6T layer. In the absorption maximum at 571 nm, assigned to the π–π^* (HOMO → LUMO) transition of the conjugated electron system, the ratio $k_{\text{in-plane}}/k_{\text{out-of-plane}}$ is 4.1 (Table 1). Applying Eq. (5) the corresponding extinction coefficients result in an orientation order parameter $S = -0.34$. Assuming that the transition dipole is parallel to the molecular long axis, this indicates a prevalently lying (horizontal) orientation of the DCV6T molecules on the substrate. The corresponding average tilt angle θ is $70.7° \pm 2.0°$ as derived from Eq. (5). While this value indicates the average of the distribution of all individual molecular tilt angles, the development of the distribution itself cannot be derived from the measured values. Interestingly, we find these results are also corresponding well to findings of X-ray diffraction (XRD) and reflection measurements performed on DCV6T thin films in Ref. [26]. There, the presence of molecular orientation with nearly the same tilt angle, i.e. a tilt angle of 18.8° in respect to the substrate plane, was confirmed within the observed crystal phase. However, we like to emphasize that in contrast to XRD VASE probes all molecules no matter whether they are in the crystal or amorphous phase. After annealing of the sample D at 90 °C for 120 min under argon atmosphere, we observe a change in the optical constants as presented in Fig. 4 (right). The anisotropy is even more pronounced, displayed by an increase of the birefringence at 1200 nm to $\Delta n = 0.204$, and an increase of the $k_{\text{in-plane}}/k_{\text{out-of-plane}}$ peak ratio to 8.9 concomitant to the change of the orientation order parameter S to −0.42. This means, that by reorganization during the annealing process the DCV6T molecules adopt a higher parallel to the substrate order than in the as produced sample. The average tilt angle θ increases to $76.6° \pm 2.6°$. Increasing the annealing temperature to 120 °C did not further influence the optical characteristics.

Besides the optical properties also the surface topology of sample D is investigated by AFM. Results are shown in Fig. 5 compared to the topology measured on the substrate surface itself. In both cases the DCV6T layer is very smooth, with a root mean square (RMS) roughness of 0.7 and 1.2 nm for the as produced and annealed sample D, respectively. The small increase may be related to the reordering of molecules during annealing. However, the roughness is still small enough to ensure high quality of the ellipsometric measurement.

The observed prevalently horizontal alignment of the DCV6T molecules on the substrate is different from studies of other sexithiophene (6T) derivatives like α-6T or α,ω-dihexyl-6T (DH6T), which tend to adopt a standing molecular orientation on the substrate [27–29]. We suggest, that the DCV end groups and the butyl side chains hinder strong interaction between the thiophene cores and therefore a more horizontal alignment on the substrate is preferred. Similar behavior has been reported by Yokoyama et al. with bis-styrylbenzene derivatives of linear shape having carbazole or diphenylamine groups at both ends [30]. It is worth noting that the horizontal orientation of the DCV6T molecules is beneficial for the use in organic solar cells due to the optimal interaction with the incident light. As is shown by Levichkova et al. [14], already very thin layers of DCV6T (e.g. 10 nm) can thus be utilized in flat heterojunction solar cells to efficiently harvest the light. The investigations furthermore show that annealing can help to achieve a more horizontal orientation, thereby the maximum value of the extinction coefficient increases by about 4% from $k_{\max} = 0.867$ (sample D, as produced) to $k_{\max} = 0.903$ (sample D, annealed). This seems rather small but may still play a considerable role in solar cells, since higher absorption directly increases the obtained short

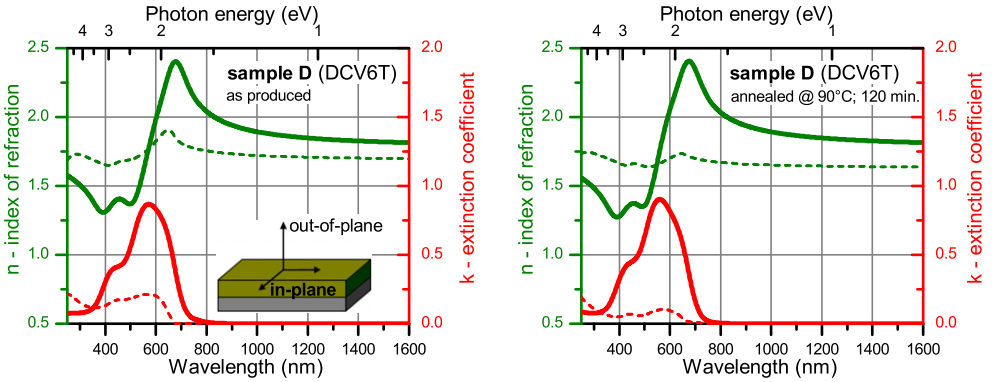

Fig. 4. Anisotropic optical constants of DCV6T measured in sample D, i.e. on interference enhanced substrate (left). The respective Ψ and Δ data of the fit and measurement are shown in Fig. 3. The optical constants of the very same DCV6T layer after annealing at 90 °C for 120 min are shown in the right graph. The inset shows the direction of in-plane (thick lines) and out-of-plane (thin dashed lines) optical constants.

Table 1
Overview about the results of the ellipsometric investigations, showing the birefringence (Δn), measured at 1200 nm, the ratio of the extinction coefficients measured at the DCV6T peak absorption, and the MSE values, applying either isotropic or uniaxial anisotropic Cauchy models in the wavelength range of 1000–1680 nm for samples D and F. MSE values given in brackets denote the results achieved by oscillator models covering the complete measured wavelength range of 245–1680 nm. In sample F the orientation parameter cannot be evaluated since the peak absorption also contains contributions from C60, which is considered isotropic.

Sample	Material	Δn (@1200 nm)	S (@ peak)	$k_{\text{in-plane}}/k_{\text{out-of-plane}}$(@ peak)	MSE – isotropic	MSE – anisotropic
D	DCV6T	0.139	−0.34	4.1	49.60	21.00
$D_{annealed}$	DCV6T	0.204	−0.42	8.9	55.41	16.95
F	DCV6T:C60	0.055	–	2.0	10.74 (54.43)	10.50 (12.89)
$F_{annealed}$	DCV6T:C60	–	–	–	11.96 (18.28)	11.71 (16.43)

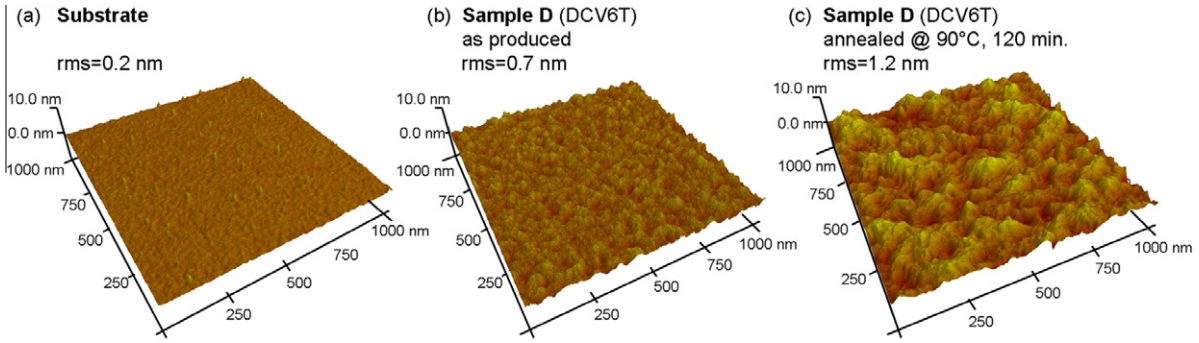

Fig. 5. AFM images of the different sample surfaces. Image (a) shows the pure substrate, (b) neat DCV6T layer and (c) the same DCV6T layer after annealing at 90 °C for 120 min. The RMS roughness values are given in the legend.

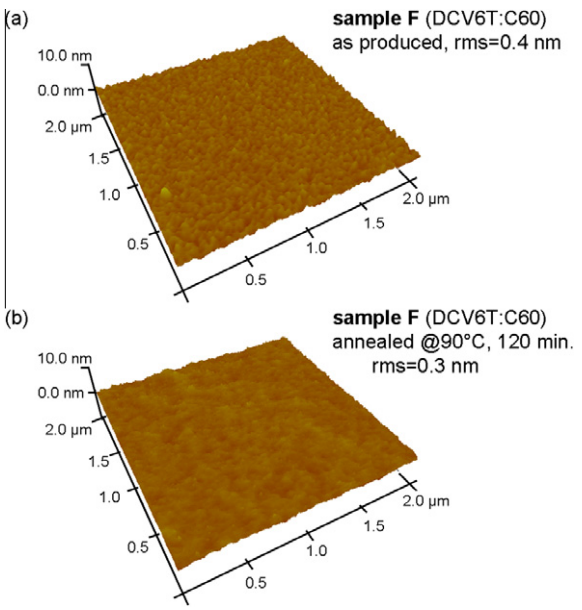

Fig. 6. AFM images of the sample F comprising a mixed DCV6T:C60 layer. Image (a) shows the as produced sample while image (b) is taken after annealing of the very same layer at 90 °C for 120 min. The RMS roughness values are given in the legend.

circuit current. In this respect, our results match to observations reported in [14], showing good solar cell performance in flat heterojunction DCV6T/C60 solar cells. In particular, they reported a higher molecular order observed by XRD, and a gain in photocurrent coming from increase of DCV6T absorption, when using layer deposition at 90 °C substrate temperature. We attribute this absorption increase to the same effect as present with annealing, i.e. the increase in the orientation order of DCV6T leads to enhanced horizontal alignment and thus higher absorption of the in-plane light component. However, the amount of orientation change might differ between the two methods.

4.3. Mixed layers DCV6T:C60

In sample F we investigate the optical properties of a mixed DCV6T:C60 layer. For better comparison the optical constants of a pure C60 layer, measured in sample E, are shown in Fig. 7. We note that due to the symmetry of the molecule itself the C60 layer is isotropic. The spectrum resembles the results already published [31,32], and shows strong absorption features at 270 nm (4.59 eV) and 346 nm (3.58 eV).

In Fig. 8 (left) the optical constants of the mixed DCV6T:C60 layer, as evaluated from the ellipsometric measurement of sample F, is presented. In the first place we did not observe strong indications for optical anisotropy by applying Cauchy model in the transparent regime, since the anisotropic approach resulted in MSE = 10.50 while the isotropic reached MSE = 10.74 (see Table 1). However, when we tried to apply the oscillator model in the full measured range of 245–1680 nm introduction of anisotropy was necessary to attain an adequate fit of the measured Ψ and Δ values and we finally came to the result

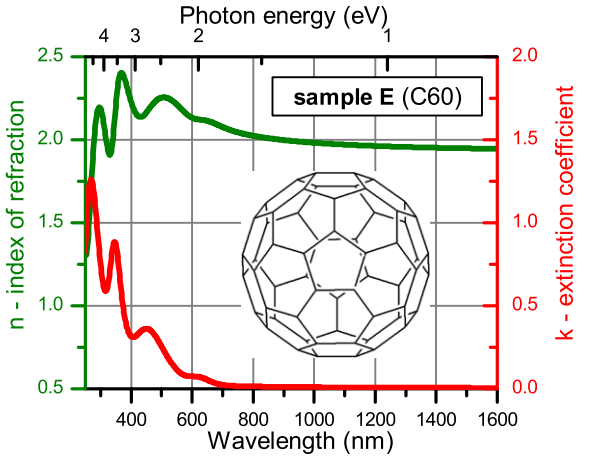

Fig. 7. Isotropic optical constants of C60 measured in sample E.

given in Fig. 8 with an MSE = 12.89 while the isotropic approach only reached MSE = 54.43 (see Table 1). The birefringence $\Delta n = 0.055$ at 1200 nm is quite low. Nevertheless, in the range of 400–700 nm, where mainly DCV6T is absorbing, the out-of-plane extinction coefficient is significantly reduced compared to the in-plane extinction coefficient and thus designates optical anisotropy. In contrast, at wavelength below 400 nm, dominated by the strong absorption features of C60, the in-plane and out-of-plane extinction components are identical. While isotropic behavior of the C60 related absorption features is expected, the observed anisotropy in the features related to DCV6T indicate that the DCV6T molecules adopt a preferential orientation with their long axis rather parallel to the substrate plane similar to the results of the pure DCV6T layer (see Fig. 4). However, the ratio $k_{\text{in-plane}}/k_{\text{out-of-plane}}$ at the peak absorption is only 2.0 compared to 4.1 in the pure layer (see Table 1). We do not evaluate the orientation parameter S here, because the small contribution of C60 still present in the range of the main DCV6T absorption can hardly be separated and therefore the parameter S would not give adequate results. Nevertheless, comparison of the spectra and the $k_{\text{in-plane}}/k_{\text{out-of-plane}}$ ratios suggests that the preferentially lying orientation of DCV6T is not as well pronounced as in case of the pure layer. Thus we conclude that the presence of C60 in the mixed layer hinders the constitution of highly ordered DCV6T.

It shall be noted that we have also tried modeling approaches, where the individual optical constants of DCV6T and C60 are mixed via an effective medium approach (EMA). This model has for example been used by several authors for blends of poly(3-hexylthiophene) and phenyl-C61-butyric methyl ester to investigate vertical composition gradients [33,34]. For the material system DCV6T:C60 investigated here, such model approaches failed to provide a good fit to the measured data. It turned out that the individual optical constants derived from the neat layers are not adequately describing the response of the materials when mixed together. Especially in case of DCV6T it can already be seen from the results given above, that the absorption strength of in-plane and out-of-plane components, i.e. the ratio $k_{\text{in-plane}}/k_{\text{out-of-plane}}$, differs when going from a pure DCV6T layer to the mixed layer. Since this change, related to the changes in degree of orientation order, is not accounted for by the EMA model it is not a well suited model for the system under investigation. As also stated by other authors [32,35], we recommend checking the suitability of the EMA models very carefully, especially when vertical composition gradients are investigated.

After investigation of the sample F, it has in a next step been annealed at 90° for 120 min and was measured again. The optical constants, as evaluated from the ellipsometric measurement, are given in Fig. 8 (right). In Table 1 the corresponding MSE values for isotropic and anisotropic model approaches are presented. Surprisingly we found, that the measured data can be described well with the isotropic oscillator model giving MSE = 18.28, while the anisotropic one reaches MSE = 16.43. Furthermore, the resulting optical constants from the anisotropic approach do not show any anisotropic features but in-plane and out-of-plane extinction coefficients are mainly concurrent over the full spectral range. Therefore, we conclude that the sample is rather isotropic after the annealing procedure. In Fig. 6 AFM images of sample F before and after annealing are

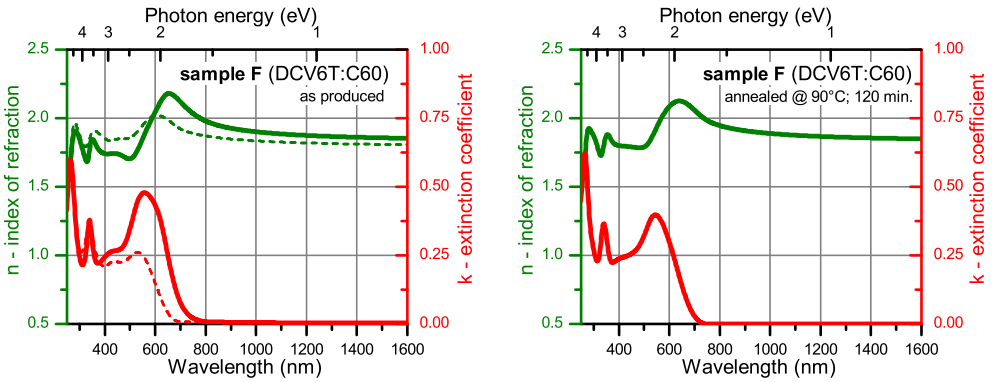

Fig. 8. Optical constants of the mixed layer DCV6T:C60 measured in sample F, i.e. on interference enhanced substrate (left). The difference in in-plane (thick lines) and out-of-plane (thin dashed lines) optical constants denotes the anisotropic behavior. The optical constants of the very same layer after annealing at 90 °C for 120 min are shown in the right graph and were found to be isotropic.

shown. In both cases the surface is very smooth with RMS-roughness below 1 nm. Thus, a high quality of the ellipsometric measurement is given in both cases.

When comparing the optical constants of DCV6T:C60 in the as produced and annealed case, we find no change in the extinction of the C60 related absorption features (270 and 346 nm). However, in the range above 400 nm, where DCV6T is mainly absorbing, the (isotropic) extinction spectrum after annealing lies in between the values of the in-plane and out-of-plane extinction spectra measured at the as produced sample, which exhibits optical anisotropy. We conclude that during the mixed layer growth the DCV6T molecules orient their long axis preferentially parallel to the substrate, i.e. parallel to the surface plane they are deposited onto, because of the weak interaction between DCV6T pairs [30]. In comparison, for α-6T showing strong π–π interaction between molecular pairs strong crystallization with preferred vertical orientation, which is detrimental for solar cell application, has been reported in films mixed with C60 [36]. In this respect, DCV6T is better suited, since molecular interaction is sterically hindered by the additional end and side groups, such that preferential lying orientation can be achieved in the mixed layer. However, it seems that this is an effect that comes only with the growth, since this preferential orientation is lost after annealing. We suggest that annealing induces a molecular reorganization process, where the DCV6T molecules choose convenient orientations in respect to the direct molecular surrounding but without preferences provided by the substrate or surface plane any more. Thus, the DCV6T molecules adopt rather randomly tilted orientations, while both C60 and DCV6T are reorganized. This leads to the observed transition from optical anisotropic behavior to isotropic behavior. As a consequence, the absorption of light, which is generally of perpendicular incidence and thus couples to the in-plane extinction, is reduced as this extinction coefficient is found to be higher in the as produced case than after annealing. This is an important result for solar cells, especially when considering that moderate annealing is part of the daily life cycle. In sample F the maximum extinction coefficient assigned to DCV6T decreases by ca. 17% from 0.478 to 0.398 during annealing. This reduction of in-plane absorption would directly lead to reduction of photocurrent in solar cells. However, during annealing the increase of short range order and crystallinity as well as higher phase separation are also expected, which are in return positive effects for solar cell performance [17,37,38]. These effects might outweigh the loss of absorption and lead to solar cells with higher efficiency [13]. Furthermore, annealing of a complete solar cell stack may give different results than seen here, due to the presence of a top metal layer [39]. In fact, we have seen growing of additional slab-like features (with height of 10–40 nm and width of 100–200 nm) on the surface when annealing temperatures of 120 °C were used, indicating that the investigated mixed layer is not in the thermodynamically most stable state. Therefore, we need to investigate the detailed morphological effects further by additional XRD measurements and other techniques.

5. Summary

In summary, the VASE results of sample A, B, C without thick SiO_2 layer as compared to the results of sample D comprising a 964 nm thick SiO_2 layer for interference enhancement shows that the uniqueness of the fit result is significantly improved and parameter correlations are reduced by applying this interference enhancement technique. Also with higher thickness of the investigated layer, the uniqueness of the result is improved. This technique is especially valuable when anisotropic materials are tested, and thus many parameters have to be used.

The investigation of DCV6T, which is a good performing donor material in solar cells, revealed that in neat layers the molecules have a prevalently lying orientation with the long axis parallel to the substrate plane. This is indicated by a ratio $k_{\text{in-plane}}/k_{\text{out-of-plane}} = 4.1$, and an orientation order parameter $S = -0.34$ at the absorption peak wavelength. After annealing of the layer at 90 °C for 120 min the molecules get even better ordered and $k_{\text{in-plane}}/k_{\text{out-of-plane}} = 8.9$ and $S = -0.42$ are achieved, i.e. the optical anisotropy is further enhanced. The lying on the substrate orientation ensures high absorption in solar cells, because the incident light can interact well with the molecular transition dipole. This result explains why DCV6T is better suited for OSC than, e.g. materials like 6T or DH6T, which tend to adopt a standing on the substrate orientation.

We show that also in mixed layers of DCV6T:C60 a preferentially lying orientation of DCV6T molecules is discovered by ellipsometry. This anisotropy of the DCV6T component in the mixed layer is indicated by a small birefringence and by diverging extinction coefficients in the wavelength range above 400 nm, where DCV6T is mainly absorbing. However the ratio $k_{\text{in-plane}}/k_{\text{out-of-plane}}$ only reaches 2.0 and is thus lower than in the neat layer case, showing that the presence of C60 hinders high ordering of the DCV6T. After annealing of the mixed layer at 90 °C for 120 min the whole sample shows optical isotropic behavior, indicating that the orientation order achieved directly after deposition is lost during the reorganization of the molecules. This effect is very important for solar cell application since annealing is often used during production processes and is also part of the daily life cycle. Therefore, future work is needed to clarify this effect.

Finally, we have shown that VASE is a valuable method for characterization of absorber materials used in OSC, providing information about optical constants as well as anisotropic behavior and molecular orientation. In general, VASE measurements may also serve for investigations of materials utilized in other organic electronic applications, where optical properties and/or molecular orientation are relevant for performance improvement.

Acknowledgments

We like to thank Neha Singh from J.A. Woollam Co., Inc. for fruitful discussions and her valuable ideas. We furthermore acknowledge technical support by Roland Schulze. This work was co-funded by the Free State of Saxony and

the European Union via the European Regional Development Fund (ERDF) under SAB Project Number 71070.

References

[1] H.E. Katz, J. Huang, Annual Review of Materials Research 39 (2009) 71.
[2] B. Maennig, J. Drechsel, D. Gebeyehu, P. Simon, F. Kozlowski, A. Werner, F. Li, S. Grundmann, S. Sonntag, M. Koch, K. Leo, M. Pfeiffer, H. Hoppe, D. Meissner, N.S. Sariciftci, I. Riedel, V. Dyakonov, J. Parisi, Applied Physics A-Materials Science & Processing 79 (2004) 1.
[3] M. Riede, T. Mueller, W. Tress, R. Schueppel, K. Leo, Nanotechnology 19 (2008) 424001.
[4] G. Horowitz, Advanced Materials 10 (1998) 365.
[5] Y.M. Sun, Y.Q. Liu, D.B. Zhu, Journal of Materials Chemistry 15 (2005) 53.
[6] S. Reineke, F. Lindner, G. Schwartz, N. Seidler, K. Walzer, B. Lussem, K. Leo, Nature 459 (2009) 234.
[7] K. Walzer, B. Maennig, M. Pfeiffer, K. Leo, Chemical Reviews 107 (2007) 1233.
[8] D. Yokoyama, A. Sakaguchi, M. Suzuki, C. Adachi, Applied Physics Letters 93 (2008) 173302.
[9] D. Yokoyama, A. Sakaguchi, M. Suzuki, C. Adachi, Applied Physics Letters 95 (2009) 243303.
[10] D. Yokoyama, Y. Setoguchi, A. Sakaguchi, M. Suzuki, C. Adachi, Advanced Functional Materials 20 (2010) 386.
[11] K. Sahre, K.J. Eichhorn, F. Simon, D. Pleul, A. Janke, G. Gerlach, Surface and Coatings Technology 139 (2001) 257.
[12] K. Hinrichs, D. Tsankov, E.H. Korte, A. Roseler, K. Sahre, K.J. Eichhorn, Applied Spectroscopy 56 (2002) 737.
[13] D. Wynands, M. Levichkova, K. Leo, C. Uhrich, G. Schwartz, D. Hildebrandt, M. Pfeiffer, M. Riede, Applied Physics Letters 97 (2010) 073503.
[14] M. Levichkova, D. Wynands, A.A. Levin, K. Walzer, D. Hildebrandt, M. Pfeiffer, V. Janonis, M. Pranaitis, V. Kazukauskas, K. Leo, M. Riede, Organic Electronics 12 (2011) 2243.
[15] D. Wynands, M. Levichkova, M. Riede, M. Pfeiffer, P. Baeuerle, R. Rentenberger, P. Denner, K.J. Leo, Journal of Applied Physics 107 (2010) 014517.
[16] S. Pfuetzner, J. Meiss, A. Petrich, M. Riede, K. Leo, Applied Physics Letters 94 (2009) 253303.
[17] J. Sakai, T. Taima, T. Yamanari, K. Saito, Solar Energy Materials and Solar Cells 93 (2009) 1149.
[18] A.C. Mayer, M.T. Lloyd, D.J. Herman, T.G. Kasen, G.G. Malliaras, Applied Physics Letters 85 (2004) 6272.
[19] R.M.A. Azzam, N.M. Bashara, Ellipsometry and Polarized Light, Elsevier Science Ltd., 1987.
[20] H. Fujiwara, Spectroscopic Ellipsometry: Principles and Applications, John Wiley & Sons, 2007.
[21] C.M. Ramsdale, N.C. Greenham, Advanced Materials 14 (2002) 212.
[22] J.N. Hilfiker, N. Singh, T. Tiwald, D. Convey, S.M. Smith, J.H. Baker, H.G. Tompkins, Thin Solid Films 516 (2008) 7979.
[23] M. Campoy-Quiles, J. Nelson, P.G. Etchegoin, D.D.C. Bradley, V. Zhokhavets, G. Gobsch, H. Vaughan, A. Monkman, O. Inganas, N.K. Persson, H. Arwin, M. Garriga, M.I. Alonso, G. Herrmann, M. Becker, W. Scholdei, M. Jahja, C. Bubeck, Physica Status Solidi C 5 (2008) 1270.
[24] O.D. Gordan, T. Sakurai, M. Friedrich, K. Akimoto, D.R.T. Zahn, Organic Electronics 7 (2006) 521.
[25] M. Campoy-Quiles, P.G. Etchegoin, D.D.C. Bradley, Synthetic Metals 155 (2005) 279.
[26] A. Levin, M. Levichkova, D. Hildebrandt, M. Klisch, A. Weiss, D. Wynands, C. Elschner, M. Pfeiffer, K. Leo, M. Riede, Thin Solid Films, in press. doi:10.1016/j.tsf.2011.10.022.
[27] B. Servet, S. Ries, M. Trotel, P. Alnot, G. Horowitz, F. Garneir, Advanced Materials 5 (1993) 461.
[28] F. Garnier, A. Yassar, R. Hajlaoui, G. Horowitz, F. Deloffre, B. Servet, S. Ries, P. Alnot, Journal of the American Chemical Society 115 (1993) 8716.
[29] S. Nagamatsu, K. Kaneto, R. Azumi, M. Matsumoto, Y. Yoshida, K. Yase, Journal of Physical Chemistry B 109 (2005) 9374.
[30] D. Yokoyama, A. Sakaguchi, M. Suzuki, C. Adachi, Organic Electronics 10 (2009) 127.
[31] A. Richter, J. Sturm, Applied Physics A-Materials Science & Processing 61 (1995) 163.
[32] D. Datta, V. Tripathi, P. Gogoi, S. Banerjee, S. Kumar, Thin Solid Films 516 (2008) 7237.
[33] M.V. Madsen, K.O. Sylvester-Hvid, B. Dastmalchi, K. Hingerl, K. Norrman, T. Tromholt, M. Manceau, D. Angmo, F.C. Krebs, Journal of Physical Chemistry C 115 (2011) 10817.
[34] M. Campoy-Quiles, T. Ferenczi, T. Agostinelli, P.G. Etchegoin, Y. Kim, T.D. Anthopoulos, P.N. Stavrinou, D.D.C. Bradley, J. Nelson, Nature Materials 7 (2008) 158.
[35] S. Engmann, V. Turkovic, G. Gobsch, H. Hoppe, Advanced Energy Materials, 1 684.
[36] J. Sakai, T. Taima, K. Saito, Organic Electronics 9 (2008) 582.
[37] P. Peumans, S. Uchida, S.R. Forrest, Nature 425 (2003) 158.
[38] T. Osasa, S. Yamamoto, M. Matsumura, Advanced Functional Materials 17 (2007) 2937.
[39] H.J. Kim, J.H. Park, H.H. Lee, D.R. Lee, J.J. Kim, Organic Electronics 10 (2009) 1505.